THE ASTROPHYSICAL JOURNAL, 403:239–248, 1993 January 20

SURVEY OF ULTRA–HIGH-ENERGY GAMMA-RAY EMISSION IN THE MAGELLANIC CLOUDS

W. H. ALLEN,[1] I. A. BOND,[2,3] E. BUDDING,[1] M. J. CONWAY,[2] A. DANIEL,[2] K. B. FENTON,[4] H. FUJII,[5] Z. FUJII,[6] N. HAYASHIDA,[7] K. HIBINO,[7] M. HONDA,[7] J. E. HUMBLE,[4] S. KABE,[5] K. KASAHARA,[8] T. KIFUNE,[7] G. D. LYTHE,[2] A. MASAIKE,[9] Y. MATSUBARA,[6] K. MITSUI,[7] Y. MIURA,[5] M. MORI,[5] Y. MURAKI,[6] M. NAGANO,[7] T. NAKAMURA,[9] M. NISHIZAWA,[10] P. M. NORRIS,[2] S. OGIO,[11] To. SAITO,[7] M. SAKATA,[10] H. SATO,[9] H. M. SHIMIZU,[5] M. SPENCER,[2] J. R. STOREY,[2] T. TANIMORI,[11] M. TESHIMA,[7] S. TORII,[8] A. WADSWORTH,[1] Y. WATASE,[5] M. D. WOODHAMS,[2] Y. YAMAMOTO,[10] P. C. M. YOCK,[2] AND T. YUDA[7]

(THE JANZOS COLLABORATION)

Received 1992 May 15; accepted 1992 July 21

ABSTRACT

Various objects in the Magellanic Clouds were monitored for ultra–high-energy (UHE) gamma-ray emission during 1988 and 1990 using Cerenkov technique at large zenith angles with the JANZOS facility. During 1990 the equipment was modified to allow a sky coverage of 7° × 23° at large zenith angles. This enabled most of the extent of the Large Magellanic Cloud to be surveyed at ultra-high energies. An examination of the data base yielded no clear eivdence for persistent UHE emission from SN 1987A and selected X-ray pulsars in the Magellanic Clouds. Upper limits on the UHE fluxes (in cm^{-2} s^{-1}) above the given threshold energies were obtained as follows: SMC X-1, 2.6×10^{-13} (>30 TeV); SN 1987A, 3.8×10^{-13} (>65 TeV); PSR 0540−693, 3.7×10^{-13} (>65 TeV); A0538−66, 1.1×10^{-13} (>130 TeV); LMC X-4, 3.5×10^{-13} (>140 TeV). We then examined the data base for pulsed UHE emission from PSR 0540−693 at the well-determined X-ray period (50 ms); and for the X-ray binary systems SMC X-1 and LMC X-4, we carried out pulsar periodicity searches on a night-by-night basis near their respective X-ray periods. No statistically significant evidence for pulsed UHE emission was found for these objects. The data base was further examined for evidence of previously undetected UHE sources in the Magellanic Clouds, and no significant DC excesses were found. Finally, we obtained upper limits on the UHE gamma-ray emission from these galaxies as a whole of 1.9×10^{-12} cm^{-2} s^{-1} msr^{-1} (>30 TeV) for the SMC and 1.8×10^{-13} cm^{-2} s^{-1} msr^{-1} (>65 TeV) for the LMC.

Subject headings: binaries: close — gamma rays: observations — Magellanic Clouds

1. INTRODUCTION

The Magellanic Clouds contain several objects, including supernova remnants and X-ray binaries, worthy of study at very high (~1 TeV) and ultra-high (~100 TeV) gamma-ray energies. Supernova remnants provide potential environments for high-energy gamma-ray production where the ejecta provides a target for accelerated particles. These particles may obtain their energy from the rotation of a fast-spinning magnetized neutron star (Gunn & Ostriker 1969; Goldreich & Julian 1969). It has been suggested that a recently formed neutron star in a supernova event provides particularly favorable conditions for the production of ultra–high-energy (UHE) gamma rays (Sato 1977; Berezinsky & Prilutsky 1978; Nakamura, Yamada, & Sato 1987). Alternatively, particles accelerated to lower energies can be magnetically trapped inside the shock front formed by the collision of the ejecta with the interstellar medium. This stored energy may be slowly leaked through occasional hadronic collisions producing a steady very high energy (VHE) gamma-ray flux (Cheng et al. 1990), or it may be released suddenly through Rayleigh-Taylor instabilities producing transient emission (Berezinsky & Stanev 1989). In supernova remnants, shock acceleration may also take place in the outer ejecta (Blandford & Ostriker 1978; Bell 1978a, b). This mechanism has been applied to explain the possible TeV transient observed in SN 1987A (Bond et al. 1988), where this process takes place through an encounter of the shock front with a circumstellar cloud (Honda, Terasawa, & Sato 1989).

Two supernova remnants were studied in this work, SN 1987A and PSR 0540−693. Both are in the Large Magellanic Cloud. SN 1987A presents an interesting case with the detection of a possible VHE gamma-ray transient (Bond et al. 1988) approximately coincident with an X-ray flare observed by *Ginga* (Makino 1988). The 50 ms pulsar PSR 0540−693 was discovered by *Einstein* and identified with a Crab-like supernova remnant (Seward, Harnden, & Helfand 1984).

X-ray binary systems containing a neutron star are also considered potential sources of VHE and UHE gamma rays. In this situation the energy source derives from accretion. In the unipolar induction model of Chanmugam & Brecher (1985), the neutron star magnetic field coupled with a differentially rotating accretion disk generates a potential difference across the disk where particle acceleration takes place. In the model of Cheng & Ruderman (1989), particle acceleration takes place

[1] Carter National Observatory of New Zealand, Wellington, New Zealand.
[2] Department of Physics, University of Auckland, New Zealand.
[3] Present address: Institute of Physical and Chemical Research, Wako, 351-01, Japan.
[4] Department of Physics, University of Tasmania, Hobart 7001, Australia.
[5] National Laboratory for High Energy Physics (KEK), Tsukuba 305, Japan.
[6] Cosmic Ray Section, STE Laboratory, Nagoya University, Nagoya 464, Japan.
[7] Institute for Cosmic Ray Research, University of Tokyo, Tokyo 188, Japan.
[8] Department of Physics, Kanagawa University, Yokohama 221, Japan.
[9] Department of Physics, Kyoto University, Kyoto 606, Japan.
[10] Department of Physics, Konan University, Kobe 658, Japan.
[11] Department of Physics, Tokyo Institute of Technology, Tokyo 152, Japan.

closer to the neutron star between charge-separated zones formed if the inner accretion disk rotates more rapidly than the neutron star.

The Magellanic Clouds contain three particularly interesting X-ray binaries. LMC X-4 is an X-ray pulsar with a period of 13.5 s in a binary orbit of 1.4 days. Evidence for UHE gamma-ray emission within a narrow orbital phase range (0.9–0.95) was reported by Protheroe & Clay (1985). Based on later observations with the SUGAR detector, Meyhanden et al. (1992) report evidence for neutral particle emission above 200 PeV within narrow orbital phase ranges of width 0.1 and centered at 0.15 and 0.65. Observations at very high gamma-ray energies initially showed evidence for pulsed emission between orbital phases 0.5 and 0.7, but this was not confirmed in subsequent observations (Brazier et al. 1990). SMC X-1 is a 0.7 s X-ray pulsar in a 3.9 day binary orbit and is one of the most powerful emitters among the known X-ray binaries. Preliminary results from the Durham group suggest that SMC X-1 may also be a powerful emitter of VHE gamma rays (Chadwick, McComb, & Turver 1990). The third interesting object is the transient X-ray binary system A0358−66 discovered by the *Ariel 5* satellite (White & Carpenter 1978). An X-ray pulsation period of 69.2 ms was discovered by *Einstein*, making this the fastest X-ray pulsar known to be in a binary system (Skiner et al. 1982). No evidence for this pulsar has been found at optical wavelengths (Corbet et al. 1985), and to date no VHE or UHE observations have been reported.

Another motivation for studying UHE emission from the Magellanic Clouds lies in the possibility of studying the interaction of the gamma-ray photons wtih the microwave background. The resultant absorption dip in the UHE spectrum at around 10^{15} eV has been well known for some time (Gould & Schreder 1966; Jelley 1966; Gould & Rephaeli 1978) but has not been observed. Detailed studies have shown that the depth of the dip depends critically on the distance to the source and the strength of the intervening magnetic field (Protheroe 1986; Honda 1989). Potential UHE sources in the Magellanic Clouds are at an appropriate distance for the possible detection of this feature. The mean free path for the interaction of UHE photons with microwave photons is ~10 kpc, and the distances to the Magellanic Clouds (~50 kpc to the LMC and ~60 kpc to the SMC) are large enough to ensure that a significant proportion of the UHE flux will undergo interactions before reaching Earth. However, the Magellanic Clouds are not so far away as to require incredibly powerful sources for detection.

In this paper we report the results of UHE observations targeted on the Magellanic Clouds. We employed the atmospheric Cerenkov technique, in which Cerenkov flashes of air showers produced by UHE gamma rays and cosmic rays are detected. We utilized this technique at large zenith angles. The advantages of working at large zenith angle were first pointed out by Sommers & Elbert (1987). The effective area of a Cerenkov telescope is increased because of the greater area of the Cerenkov light pool. However, because of the diminution of light intensity, the threshold energy is also increased. The large zenith angle technique was first exploited by the JANZOS collaboration, where an upper bound on the UHE gamma-ray flux from SN 1987A was obtained (Bond et al. 1989). Here we present further observations of SN 1987A and other potential sources in the Magellanic Clouds obtained during 1990 from the JANZOS experiment. We also combine the resultant data base with the data base obtained by Bond et al. in order to study UHE gamma-ray emission from these galaxies as a whole. The threshold energies for the observations reported here range from 30 TeV for SMC X-1 to 140 TeV for LMC X-4.

2. EXPERIMENT AND OBSERVATIONS

2.1. *Experiment*

The JANZOS facility is located at latitude −41°.7, longitude 173°.8 east, and altitude 1640 m on Altimarlock Mountain in the Black Birch Range in the South Island of New Zealand. The Cerenkov telescope is comprised of three mirrors arranged at the vertices of an approximately 80 m × 80 m × 80 m triangle. The mirrors are constructed of aluminum. Each has a diameter of 2 m and a focal length of 2 m. The experiment is of the "fast-timing" type whereby the arrival direction of a primary particle producing a Cerenkov flash is reconstructed from the differences of the arrival times recorded by each telescope.

The mirrors are steerable in elevation axis only and are operated in the so-called drift-scan mode. As a target object moves across the sky through its meridian passage, it is viewed successively by photomultiplier tubes set along its trajectory on the focal plane. For a given phototube, Cerenkov light emitted by an air shower is incident onto an area of 8 cm × 8 cm and is directed by aluminum light guides onto a 2 cm radius photocathode window. Each phototube views a 2°.3 × 2°.3 region of the sky. Cerenkov light is identified when three phototubes, one from each mirror viewing the same direction, see coincident signals. Two arrangements of phototubes are used, one employing 10 phototubes per mirror and one employing 28. These are shown in Figure 1. For all events, all phototubes are interrogated for pulse-height and timing information.

The photomultiplier tubes are Hamamatsu Photonics models H1531 and H1161. Both models are blue-sensitive and have a rise time cataloged at 2.6 ns. In addition, the H1531 has a high-gain GaAs first dynode. Before installation, the overall

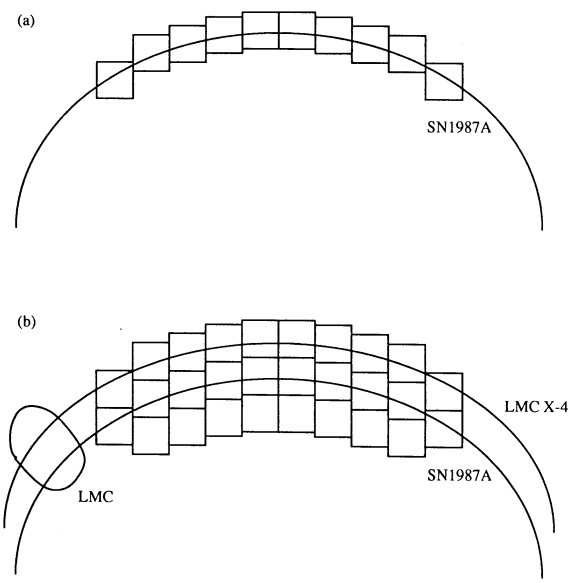

FIG. 1.—(*a*) Single-row (*b*) three-row arrangements of photomultipliers on the focal plane of one mirror of the JANZOS Cerenkov telescope. The trajectories of SN 1987A and LMC X-4 and the image of the LMC are shown.

gains were equalized by requiring equal responses when exposed to scintillation light induced by cosmic-ray muons using a reference scintillation detector. This procedure determined the supply voltages to be used, and corresponded to a nominal gain of 2×10^5, as determined by the manufacturer's specifications of gain versus voltage for the photomultipliers. After external amplification by a factor of 8.3, the outputs are fed into discriminators with thresholds set at 30 mV. This value corresponds to a discrimination level of approximately 20 photoelectrons, as determined by the known values of load resistance, gain, and pulse width of the system.

The trigger circuitry requires a triple coincidence of signals from corresponding phototubes in the three mirrors within 80 ns. To ensure that all Cerenkov signals arrive within this gate time, delay cables were added to each photomultiplier output. The lengths of these cables were specifically customized for large zenith angle observations. With this discriminator/coincidence arrrangement, Cerenkov events may be cleanly identified. For large zenith angle observations, at least 95% of observed coincidences occur for cosmic-ray–related events.

Pulse-timing measurements are achieved using time-to-digital converters (TDC) with a resolution of $\frac{1}{8}$ ns. Pulse-height measurements are achieved using analog-to-digital converters (ADC) with a resolution of $\frac{1}{4}$ pC. The absolute times of each event are recorded, at a resolution of 0.1 ms, from a standard clock controlled by a quartz oscillator.

To compensate for the variable sky background, a padding lamp system is used. A light-emitting diode (LED) is mounted near the photocathode of each phototube. The brightness of each LED is controlled by a servo-assisted negative feedback system. This maintains a constant background current at the anode of each tube regardless of any variations in the sky background. The purpose of this is to safeguard against changes in the gains of the phototubes caused by variable background current. The LED intensities were set for the present observations so that they were a little brighter than the sky in the region of the Large Magellanic Cloud. The fixed current varied from tube to tube in the range 40 to 80 μA.

2.2. *Observations*

The observations of the Magellanic Clouds which were carried out during 1988 and 1990 are summarized in Table 1. Three combinations of phototube and triggering system were employed.

1. A single row of phototubes per mirror as shown in Figure 1*a*. In this case there are 10 trigger sets of phototubes, and the field of view is 23° × 2°.3 as given by the angular extent of the phototubes. During these observations the telescopes were targeted on SN 1987A.

2. Three rows of phototubes per mirror and trigger circuitry employed on the central rows only. The field of view is the same as in combination 1, but there are more phototubes looking at Cerenkov-triggered events. During these observations the telescopes were targeted on SMC X-1.

3. Three rows of phototubes per mirror, and trigger circuitry employed in all three rows. With this setup the field of view is 23° × 7°, enabling most of the extent of the Large Magellanic Cloud to be surveyed (see Fig. 1*b*).

The Magellanic Clouds were observed at large zenith angles during their lower transits below the south Celestial pole. The SMC was observed at zenith angles around 65°, while the LMC was observed at zenith angles from 66° to 72°. The drift-scan mode allows simultaneous observations of the source and the cosmic-ray–induced background. At large zenith angles, this feature is very important. Throughout these observations no auroral activity was seen. At the Black Birch site there is no discernible artificial horizon glow toward the south. The nearest town in that direction is Kaikoura (population less than 1000) at a distance of over 100 km. The Pacific Ocean lies beyond that.

2.3. *Sensitivity*

In calculating the threshold detection energy and effective area of the apparatus, we adopt here a simple model whereby it is assumed that all Cerenkov light is emitted at shower maximum and that the integrated Cerenkov light intensity is proportional to the gamma-ray energy and independent of zenith angle. We first consider vertically incident gamma rays and calculate the threshold energy for a single mirror. This follows from the setting of the discrimination level for each photomultiplier, which was approximately 20 photoelectrons (see § 2.1 above). At this discrimination level the minimum detectable photon density at a mirror is 30 photons m^{-2}. The Hillas & Patterson (1987) density distribution for vertical showers,

$$\rho = 40\ (E/\mathrm{TeV})\ \text{photons m}^{-2}\ ,$$

then yields the threshold energy per mirror for vertically incident gamma rays, namely, 0.75 TeV. In the present experiment we require that the threshold be exceeded at all three mirrors. This yields an effective threshold energy of approximately 1 TeV, a result which is supported by detailed simulations (Lythe 1990).

The threshold for other zenith angles may be found by using the above value of 1 TeV at $\theta = 0°$ and scaling for the effects of atmospheric attenuation and increasing area of the Cerenkov light pool. We require the quantity $E_{\mathrm{th}} K/D^2 \tan^2 \xi$ to be constant as a function of zenith angle. Here K is the atmospheric attenuation factor, D is the distance from the detector to the shower maximum, and ξ is the half-angle of the Cerenkov light emitted by a particle at shower maximum. As a function of zenith angle, the attenuation is given by Hillas (1982) as

$$K = e^{-\Delta x/\Lambda}\ ,$$

TABLE 1

JOURNAL OF OBSERVATIONS OF SMC AND LMC

Observation Period	Target Galaxy	Phototube System	Trigger System	Number of Nights	Hours of Data
1988 May 13–Jul 13	LMC	Single row	Single row	16	49.0
1990 Feb 21–Apr 4	SMC	3 row	Single row	18	62.9
1990 Apr 21–Apr 22	SMC	3 row	3 row	2	10.8
1990 May 21–Jun 25	LMC	3 row	3 row	12	50.4

where

$$\Delta x = 1030 \sec\theta - x_{\max}$$

and

$$\Lambda = 1385 - 0.3798x_{\max} - 0.000556x_{\max}^2 ,$$

and the distance from the detector to shower maximum is given by Sommers & Elbert (1987) as

$$D = \left[7.1 \ln\left(\frac{1030}{x_{\max}\cos\theta}\right) - H\right] \sec\theta \text{ km} ,$$

where H is the detector's altitude in kilometers and $x_{\max}$ is the slant depth in the atmosphere where showers attain their maximum given by Greisen (1956) as

$$x_{\max} = (36 \text{ g cm}^{-2}) \ln(E/74 \text{ MeV}) .$$

Finally, ξ is given by Hillas (1982) as

$$\xi = \cos^{-1}\left(\frac{1}{n}\right) ,$$

where

$$n = 1 + 0.000296(x_{\max}\cos\theta/1030) \times 273.2/T$$

and

$$T = 204 + 0.091x_{\max}\cos\theta/103 .$$

In Figure 2 we show the threshold energy as a function of zenith angle in the range corresponding to large zenith angle observations of the Magellanic Clouds. The threshold energies range from 30 TeV for SMC X-1 to 140 TeV for LMC X-4.

In this paper we define the effective area $A(E_{\text{th}})$ in such a way that the product of this quantity and the *integral* flux above the threshold energy gives the observed number of gamma-ray events. The effective area for these observations is calculated using a similar approach to that of Sommers & Elbert (1987). Here the complicated viewing geometry introduced by three telescopes was treated by means of a Monte Carlo calculation. For a given zenith angle and spectral index γ, events were sampled at random from an $E^{-\gamma}dE$ distribution above the corresponding threshold energy. These events were then thrown at random around the vicinity of the telescope array. For each event the detectability at each telescope was tested assuming a flat-top lateral distribution of Cerenkov photons emitted by gamma-ray–initiated showers. The effective area is then determined from those events that may be viewed by all three telescopes.

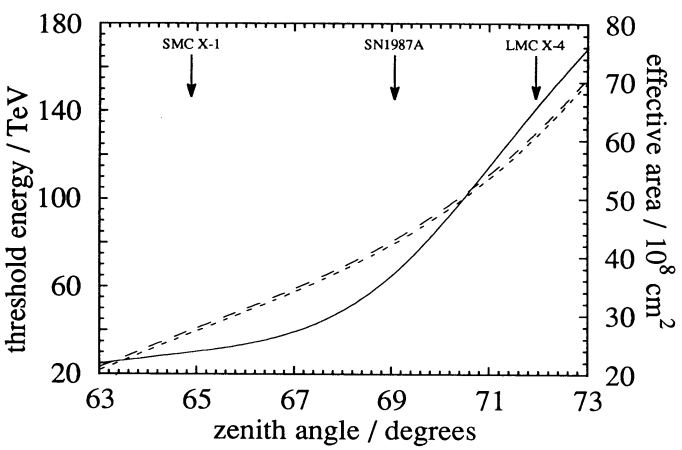

FIG. 2.—Threshold energy (*solid line*) and effective area of the JANZOS Cerenkov telescope as functions of zenith angle. The effective area is shown for differential spectral indices of −2.6 (*dashed line*) and −2.0 (*dotted line*). The range of zenith angles corresponds to observations of the Magellanic Cloud at large zenith angles.

The effective area as a function of zenith angle, calculated for a spectral index of 2.6 and 2.0, is also shown in Figure 2. The dependence on the spectral index is very weak and may be neglected. The effective area ranges from 2.7×10^9 cm^2 for SMC X-1 to 6.0×10^9 cm^2 for LMC X-4. For observations at vertical zenith angles the effective area is 1.0×10^8 cm^2. We note here that detailed Monte Carlo simulations of large zenith angle showers yielded similar values for the effective areas (Lythe 1990). The effective area for large zenith angle observations of SN 1987A is determined as 4.3×10^9 cm^2. This is smaller than the value adopted in our previous report (Bond et al. 1989) by a factor of 1.7. The original value was calculated assuming the viewing geometry of a single telescope. Here we have taken into account the viewing geometry for an array of three telescopes. The coincidence requirement would reduce the effective area from that of a single telescope.

3. DATA ANALYSIS AND ANGULAR RESOLUTION

The primary arrival direction for each event is calculated by fitting a unique plane to the times recorded by the three mirrors. For those events where multiple hits are recorded in a mirror, the time is taken from the signal of maximum amplitude. Inherent timing delays from instrumental sources (signal cable lengths, phototube electron transit time) were calibrated for each phototube using a pulsed laser optical fibre system. Additional calibration experiments were carried out by observing the transits of bright stars across the field of view of successive phototubes with the padding lamp system disabled, and measuring the associated changes in anode current. By observing various stars at different declinations, the orientation of each telescope and pointing direction of each phototube could be determined to an accuracy of 0°.2. Comparing these results with the observed distributions of events allowed us to check for systematic errors in the delay calibration. A scatter plot showing a typical distribution of arrival directions is given in Figure 3. The observations of bright stars were also used to determine the relative gains of the various photomultipliers at regular intervals to an accuracy of 20% or better.

The angular resolution of the system is determined by the accuracy of the plane approximation in reconstructing the arrival directions of observed Cerenkov events. Diffuseness and curvature in the shower front produce errors in the measured arrival directions. By diffuseness we mean here the precision with which the passage of the Cerenkov shower front through a mirror is measured. The diffuseness of the shower front was determined by looking at time differences among fired phototubes for multiple hit events. The FWHM diffuseness error was then found to be 3.6 ns. This result is based on observed events where the vast majority are proton-initiated. The diffuseness may be less for gamma-ray–initiated showers, since proton showers have several electromagnetic and hadronic subshower components (Sembioski & Kertzman 1991).

The effects of shower-front curvature on the angular resolution can be estimated using the assumption that all light is emitted at shower maximum. Simulated gamma-ray–

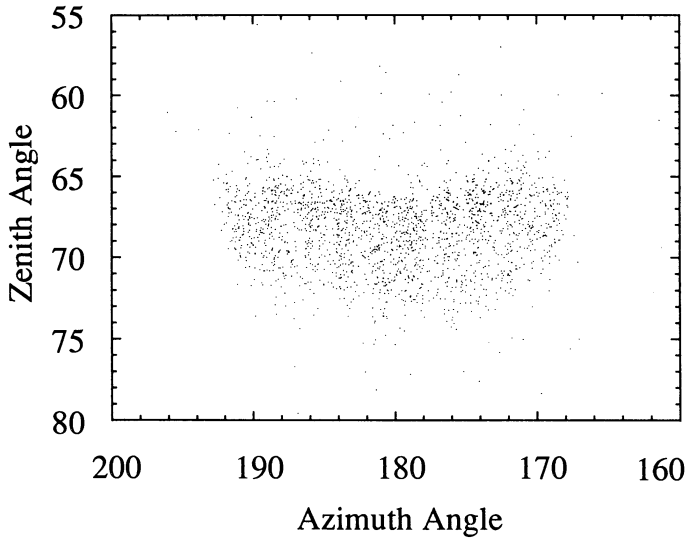

FIG. 3.—Distribution in zenith and azimuth of arrival directions of analyzed events corresponding to one night of observation of the LMC where trigger circuitry was employed on all 28 sets of three phototubes, one from each mirror. The absence of points away from the central region demonstrates that at least 95% of the events are due to air showers.

initiated showers injected at large zenith angles have a curved shower front consistent with the model (Lythe 1990). The size of the light pool in the plane perpendicular to the shower axis is defined by the half-angle, ξ, for Cerenkov radiation at the height of the shower maximum. Using the plane approximation will give an estimate of the arrival direction which points toward the shower maximum—slightly different from the true arrival direction if the core falls outside the triangle formed by three mirrors. The error introduced by this effect is less than ξ. If the core falls near the edge of the triangle, the curvature error becomes 0.8 ns in the direction of right ascension. For a baseline of 80 m this corresponds to 0°.2. In the direction of declination, the baseline of the triangle seen by the shower is smaller. The associated curvature error expressed in time units is then 0.3 ns. However, in angular units the curvature error in declination is the same as that in right ascension, i.e., 0°.2.

Combining both the diffuseness and the curvature timing errors gives an angular resolution of 0°.4 in the direction of right ascension, and in declination the resolution ranges from 0°.9 for observations of SMC X-1 to 1°.2 for observations of LMC X-4. These values dictate the optimum bin sizes to be used in searches for point sources.

4. RESULTS

4.1. *Search for DC UHE Emission from Selected Objects*

The UHE data base obtained from the 1990 observations of the Magellanic Clouds was examined for evidence of gamma-ray emission from SN 1987A and the X-ray pulsars PSR 0540−693, LMC X-4, A0538−66, and SMC X-1. For each source a 2° wide declination strip, centered on the source, was divided into 3° wide right ascension bins into which the arrival directions of observed events were distributed.

For each source observation, there are at least seven phototubes viewing the off-source directions. This feature allows the background to be well determined as follows: From the data we find two distribution functions $f(\phi)$ over hour angle, and $g(t)$ over time. The right ascension α is a function $h(\phi, t)$ of hour angle and time. The background, $B(\alpha)$, as a function of right ascension is then found by integrating the product $f(\phi)g(t)$ over all combinations of ϕ and t such that $\alpha = h(\phi, t)$, i.e.,

$$B(\alpha) = \frac{1}{N} \iint_{\alpha = h(\phi,\ t)} f(\phi)g(t)d\phi\, dt\ ,$$

where N is the number of events in the strip. This quantity is calculated separately for each trigger set viewing the strip, and the total background is then found by summing over these sets. This allows for variability among the trigger set responses caused, for example, by observing in partly cloudy conditions. With this procedure, all off-source events in the declination strip are used in the calculation of the background rate in a direction centered on a source. As a consequence of this, the background is very accurately determined, because the number of off-source events is much greater than the number of on-source events.

Given the observed distribution of events and the calculated background along the strip, one simply examines the bin centered on the source for excess events. These right ascension scans were carried out for each night of observation and summed accordingly. The results of such a scan corresponding to the total data set of observations of SN 1987A during 1990 are shown in Figure 4. In the source bin there are 2330 observed events over a background of 2275 ± 12. The excess of 55 events is significant only at the 1.1 σ level. The results of night ascension scans for SN 1987A and the other objects are summarized in Table 2. It can be seen that none of these objects show significant excess events.

Also given in Table 2 are the inferred upper limits on the integral flux and the luminosity at the 95% confidence level. These were calculated as follows, using the total observed number of events N_T and the background N_B in a source bin. Assuming Poisson statistics, the uncertainty is $N_T^{1/2}$. The uncertainty in the background is determined by the number of events in the declination strip and is given by $N_B/N^{1/2}$. These errors add in quadrature to give the uncertainty in the observed excess, $N_T - N_B$. The 95% (1.9 σ) upper limit on the number of on-source events is then

$$N_{95} = \frac{1}{f}\left[N_T - N_B + 1.9\left(\frac{N_T + N_B^2}{N_{\rm off}}\right)^{1/2}\right],$$

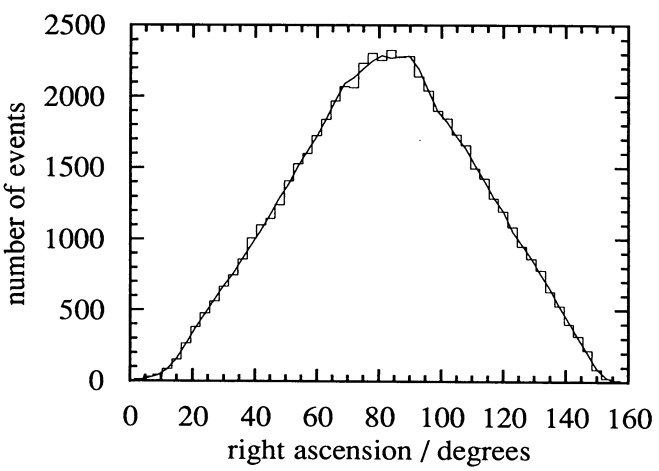

FIG. 4.—Results of a right ascension scan across the declination strip centered on SN 1987A for the total data set of observations made during 1988 and 1990. The smooth curve is the background as described in the text.

TABLE 2

UPPER LIMITS AT THE 95% CONFIDENCE LEVEL ON UHE-EMISSION-SELECTED OBJECTS IN THE MAGELLANIC CLOUDS

Object	N_T	N_B	N_{95}	Threshold Energy (TeV)	Integral Flux Upper Limit (10^{-13} cm^{-2} s^{-1})	Luminosity Upper Limit (10^{37} ergs s^{-1})
SMC X-1	2955	2946 ± 10	187	30	2.6	3.9
PSR 0540−66	3768	3680 ± 12	383	65	3.7	7.4
SN 1987A	3783	3697 ± 13	380	65	3.8	7.6
A0538−66	1074	1075 ± 6	122	130	1.1	3.8
LMC X-4	1165	1144 ± 7	171	140	3.5	6.3

where f is the fraction of events expected to fall within the bin region given the angular resolution for gamma-ray events. The integral flux limit above the threshold energy E_{th} is then

$$F(>E_{th}) < \frac{N_{95}}{A(E_{th})T},$$

where T is the total observation time after allowing for the dead time of the experiment. Given the distance D to the source and a cutoff energy E_{max}, the luminosity is given by

$$L(>E_{th}) < 4\pi D^2 \int_{E_{th}}^{E_{max}} E \frac{df}{dE} dE,$$

where the differential flux in terms of the associated index Γ may be written as

$$\frac{df}{dE} = CE^{\Gamma}.$$

The constant C may be determined by the integral flux, $F(>E_{th})$, using

$$F(>E_{th}) = K \int_{E_{th}}^{E_{max}} E^{\Gamma} dE.$$

Assuming a spectrum of differential index -2 and using an upper limit on the integral flux, the corresponding luminosity limit is then

$$L(>E_{th}) < 4\pi D^2 F(>E_{th}) \frac{E_{th} E_{max}}{E_{max} - E_{th}} \ln\left(\frac{E_{max}}{E_{th}}\right).$$

For the distances we adopt 47.8 kpc for the LMC and 57.5 kpc for the SMC (see Feast 1990 for a review of distance measures to the Magellanic Clouds).

The flux upper limits for SN 1987A, LMC X-4, and SMC X-1 are shown in Figures 5*a*–5*c* in comparison with results obtained by other experiments. Upper limits obtained by the JANZOS air-shower array between 1987 October and 1989 April are given by Bond et al. (1990) for SN 1987A and LMC X-4, and Allen et al. (1991) for SMC X-1. We have also included the detected flux for the TeV burst and the overall upper limit based on observations of the upper transit of SN 1987A with the JANZOS Cerenkov facility during 1987 December and 1988 January (Bond et al. 1988), as well as the upper limit obtained from the 1988 large zenith angle observations of SN 1987A. Upper limits on the UHE fluxes of SN 1987A, LMC X-4, and SN 1987A obtained from the South Pole Air Shower Experiment (SPASE) are given by Finnemore et al. (1991). Results obtained by other groups include upper limits for SN 1987A (Adelaide: Ciampa et al. 1988; Potchefstroom: Raubenheimer et al. 1988; Durham: Chadwick et al. 1988); an upper limit for LMC X-4 obtained by the Durham group (Brazier et al. 1990) and the flux corresponding to the PeV detection reported by Protheroe & Clay (1985); and the flux corresponding to the possible VHE detection of SMC X-1 by the Durham group (Chadwick et al. 1990). Where appropriate, all upper limits have been converted to their equivalent values at the 95% confidence level.

In the UHE range 10–1000 TeV, the upper limits for SN 1987A presented here are the most restrictive. However, the upper limit for SN 1987A of 3.8×10^{-13} cm^{-2} s^{-1} presented here is larger than that of our previous report (Bond et al. 1989). The analysis techniques here are different from those of the previous report in several respects. In this work the effective area is smaller by a factor of 1.7, the declination strip is twice as wide, and the background calculation method is slightly different in that the prescription described in § 4.1 is applied to each trigger set separately.

The upper limit for SMC X-1 is the most restrictive, while the LMC X-4 value is comparable to those obtained by the JANZOS air-shower array and by SPASE. If SMC X-1 is a persistent emitter of VHE gamma rays, then, on combining our result and the Durham result, we constrain the differential spectral index in the 0.4–30 TeV range to be steeper than -2.4.

4.2. *Search for Episodic and Pulsed Emission*

A search for episodic emission from SN 1987A, PSR 0540−693, A0538−66, LMC X-4, and SMC X-1 was carried out by inspecting the right ascension scans on a night-by-night basis. For a given object, observations on different nights are compared using the signal strength given by

$$S = \frac{N_T - N_B}{N_B}.$$

Although positive signal strengths were observed, they were not significant and are consistent with statistical fluctuations. In Figure 6 we plot the observed signal strengths as a function of observation day for the 1990 observations of SN 1987A and LMC X-4.

Since the X-ray pulse parameters of PSR 0540−693 are very well determined (Nagase et al. 1990), the 1990 data base was further scrutinized by searching from associated pulsed UHE emission from this object. This was done by means of an epoch folding technique. For each event within the source bin we calculate the X-ray phase using

$$\phi = \nu t + \tfrac{1}{2}\dot{\nu} t^2 + \tfrac{1}{6}\ddot{\nu} t^3,$$

where ν, $\dot{\nu}$, and $\ddot{\nu}$ are the X-ray pulse frequency and associated derivatives, which are taken from Nagase et al. (1990). All times are corrected to the solar system barycenter using the JPL

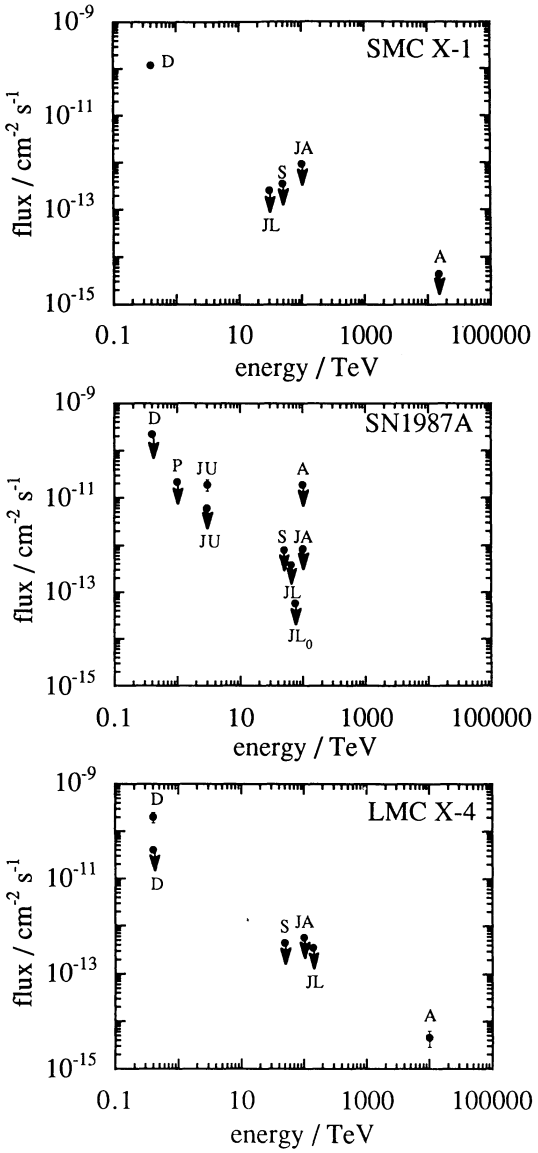

FIG. 5.—Comparison of upper limits on the UHE gamma-ray fluxes from SMC X-1, SN 1987A, and LMC X-4. The present results obtained using the JANZOS Cerenkov telescope at large zenith angles are designated as "JL". The previous upper limit on SN 1987A obtained from large zenith observations is designated as JL_0. Results from observations during the upper transit of SN 1987A using the JANZOS Cerenkov telescope at conventional zenith angles are designated as "JU." Results from analysis of the JANZOS air-shower array data from 1987 October to 1989 April are designated as "JA." Results from other groups are designated as follows: SPASE, "S"; Durham, "D"; Adelaide, "A"; and Potchefstroom, "P."

ephemeris. The phases were then distributed into bins of width 0.1. The phase histogram obtained is shown in Figure 7. The small excess seen is not localized to any one bin, thus showing that there is no detection of UHE pulsed emission at the X-ray period. PSR 0540−693 was also in the field of view during the 1988 observations. The above analysis was repeated on this data base with essentially the same result.

For the X-ray binary systems LMC X-4 and SMC X-1, pulsar periodicity searches near their respective X-ray pulse periods were carried out. As well as correcting to the solar system barycenter, all event times were further corrected to the focus of the binary orbit using the elements of Levine et al.

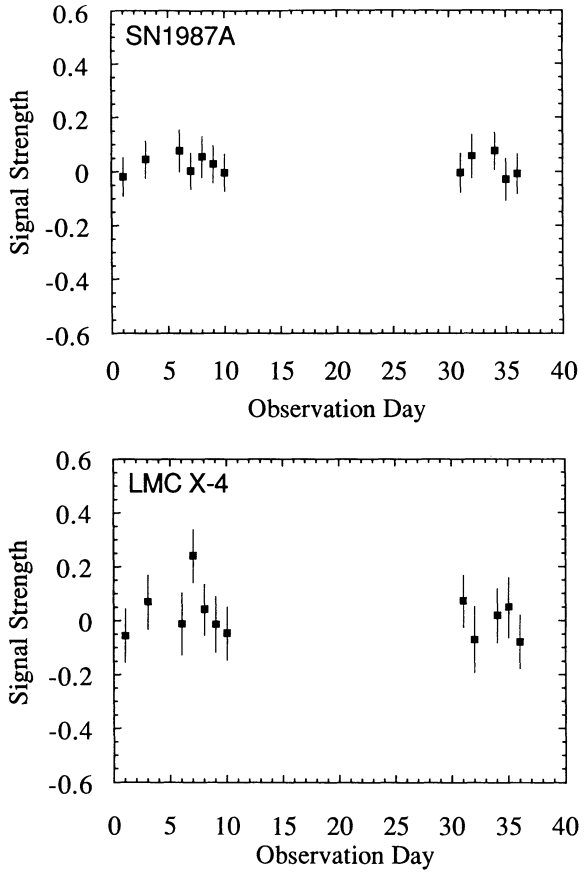

FIG. 6.—Signal strengths of excess events from the direction of SN 1987A and LMC X-4 for each night of observations during 1990. Observation day 1 corresponds to 1990 May 21.

(1991) for LMC X-4 and Primini, Rappaport, & Joss (1977) for SMC X-1. The periodicity searches were carried out on each night using the Rayleigh test, and the results were compared with any observed DC excesses.

A marginally significant result of this analysis was found in the data corresponding to the 1990 May 27 observations of

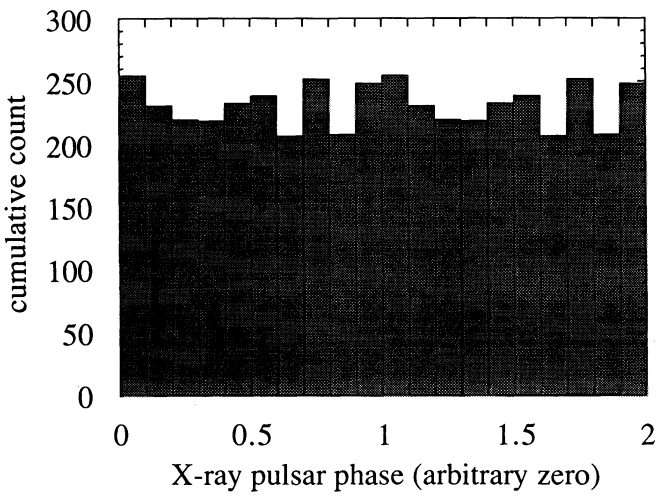

FIG. 7.—Phaseogram with respect to the X-ray pulsar phase for events in the right ascension bin centered on PSR 0540−693 for observations made during 1990.

LMC X-4. In the range 13.46–13.54 s, a Rayleigh peak corresponding to a chance probability of 0.018 occurs at 13.470 s. Inspection of the right ascension scan showed that a total of 127 events was observed in the source bin with a background of 102 on May 27. The excess of 25 events (2.2 σ using the method of Li & Ma 1983) observed on this night was the largest among the observations (see Fig. 6). Allowing for six independent trials in the test period range and for the fact that this analysis was carried for 32 nights of observations (20 for SMC X-1 and 12 for LMC X-4), the overall chance probability was estimated to be 0.0082.

4.3. *Search for Pointlike UHE Emission from the Magellanic Clouds*

In this part of the analysis we searched the data base for previously unidentified UHE gamma-ray sources in the Magellanic Clouds. The sky covered by the observations was divided into overlapping 2° wide declination strips separated by 0°.5. The centers of these strips covered the range −71°.3 to −67°.3 for the LMC observations and −75°.5 to −71°.5 for the SMC observations. Each strip was further divided into overlapping 3° wide right ascension bins separated by 1°. On each strip, a right-ascension scan analysis was performed as described above.

Figure 8 shows the resultant distribution of standard deviations in each bin above and below the background corresponding to the total data set of observations of the LMC and SMC. Both distributions are well fitted by the error function, indicating that the data are well behaved. No right ascension bin shows an excess where the standard deviation does not follow the fitted distribution function. In particular, within the Magellanic Cloud regions, no right ascension bin showed a greater than 3 σ excess over the background, either on a night-by-night basis or on their respective total data sets. Therefore, there are no right ascension bins with large excesses that cannot be attributed to being statistical in origin, and thus this data base shows no evidence for point-source UHE gamma-ray emission from the Magellanic Clouds.

4.4. *Total UHE Gamma-Ray Emission from the Magellanic Clouds*

Finally we examined the possibility that the collective emission from all potential point and diffuse origins in the Magellanic Clouds may be detectable. For this analysis we used all available data obtained in 1988 and 1990. First the LMC region was divided into three nonoverlapping declination strips of 2° width centered on $\delta = -71°.3$, $-69°.3$, and $-67°.3$. A right ascension scan analysis was then performed on each strip using 3° wide nonoverlapping right ascension bins. This procedure was also carried out for the SMC data base, in this case using two single declination strips centered at $-73°.5$ and $-71°.5$. The observed and background events, for the total observation time, for each bin are given in Table 3. The total numbers of observed and background events for the SMC region are 20,067 and 20,105, respectively. From the LMC region these values are 49,246 and 49,258, respectively. For both galaxies, the observed events are deficits with respect to the background. This data base therefore shows no evidence for collective UHE gamma-ray emission from the Magellanic Clouds.

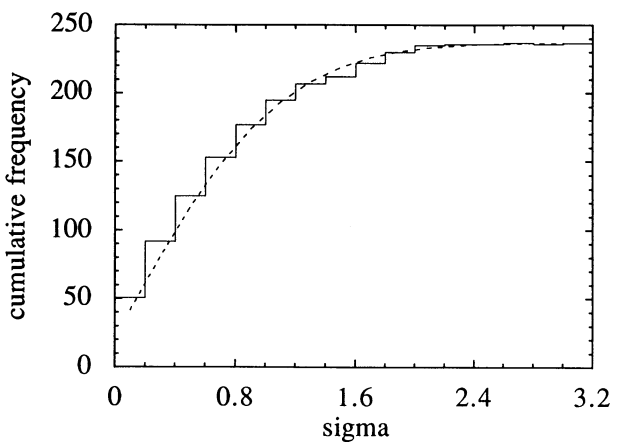

FIG. 8.—Distribution of absolute values of the standard deviations of excesses observed in right ascension bins from the total data set of LMC and SMC observations. The best-fitting error function is indicated.

Upper limits on the total UHE gamma-ray flux and luminosity per solid angle emitted by each of these galaxies were obtained as follows. In each bin within the galaxy regions, the 95% upper limit on the number of gamma-ray events was determined from the observed and background event numbers. In this case it is not necessary to allow for the effects of angular resolution. The total flux upper limit was then calculated by summing over each bin as follows:

$$F(>E_0) < \sum_i \left(\frac{E_i}{E_0}\right) \frac{N_i}{A_i T_i},$$

where E_i, A_i, and T_i are respectively the threshold energy, the effective area, and the total observation time corresponding to the ith cell. The flux limits for each cell are converted to a common threshold energy E_0 assuming an $E^{-2}\,dE$ differential spectrum. The intermediate results of this calculation are detailed in Table 3. The upper limits at the 95% confidence level on the UHE gamma-ray emission from the SMC and the LMC may be expressed as

$$F_{\rm SMC}(>E_0) < 5.8 \times 10^{-11} \left(\frac{E_0}{\rm TeV}\right)^{-1} \text{ cm}^{-2}\ \text{s}^{-1}\ \text{msr}^{-1}$$

and

$$F_{\rm LMC}(>E_0) < 1.2 \times 10^{-11} \left(\frac{E_0}{\rm TeV}\right)^{-1} \text{ cm}^{-2}\ \text{s}^{-1}\ \text{msr}^{-1}.$$

The corresponding upper limits on the luminosity may then be expressed as

$$L_{\rm SMC}(>E_0) < 2.3 \times 10^{37} \ln\left(\frac{E_{\rm max}}{E_0}\right) \text{ ergs s}^{-1}\ \text{msr}^{-1}$$

and

$$L_{\rm LMC}(>E_0) < 3.1 \times 10^{36} \ln\left(\frac{E_{\rm max}}{E_0}\right) \text{ ergs s}^{-1}\ \text{msr}^{-1},$$

where $E_{\rm max}$ is some cutoff energy. The angular sizes of the Magellanic Clouds are taken to be 1.9 msr for the SMC and 10 msr for the LMC, and the cutoff energy is taken to be 10^{17} eV. The derived upper limits are given in Table 4 using common threshold energies of 30 TeV for the SMC data and 65 TeV for the LMC data.

Fichtel et al. (1991) have theoretically calculated the cosmic-ray density distribution within the LMC based on previous observations of synchrotron radiation from this region. From

TABLE 3

RESULTS OF RIGHT ASCENSION SCAN ANALYSES FOR BINS WITHIN MAGELLANIC CLOUD REGIONS, IN THEIR RESPECTIVE DATA SETS

R.A.	Decl.	E_{th} (TeV)	Effective Area (10^8 cm^2)	Exposure Time (hr)	Observed Events	Background Events	N_{95}
			A. SMC[a]				
7°.2	−71°.5	38	33	10.8	1019	1079	2
10.2	−71.5	38	33	10.8	1099	1100	64
13.2	−71.5	38	33	10.8	1077	1088	53
16.2	−71.5	38	33	10.8	1113	1072	105
19.2	−71.5	38	33	10.8	1053	1050	67
7.2	−73.5	30	27	73.7	2933	2940	98
10.2	−73.5	30	27	73.7	2978	2960	124
13.2	−73.5	30	27	73.7	2883	2941	46
16.2	−73.5	30	27	73.7	2959	2935	129
19.2	−73.5	30	27	73.7	2953	2940	118
			B. LMC[b]				
75°.0	−71°.5	38	33	50.4	2350	2309	136
78.0	−71.5	38	33	50.4	2271	2334	31
81.0	−71.5	38	33	50.4	2364	2339	120
84.0	−71.5	38	33	50.4	2343	2343	95
87.0	−71.5	38	33	50.4	2350	2337	108
90.0	−71.5	38	33	50.4	2339	2299	135
75.0	−69.5	62	37	99.4	3571	3578	109
78.0	−69.5	62	37	99.4	3595	3614	96
81.0	−69.5	62	37	99.4	3664	3619	163
84.0	−69.5	62	37	99.4	3680	3618	179
87.0	−69.5	62	37	99.4	3651	3616	152
90.0	−69.5	62	37	99.4	3500	3516	99
75.0	−67.5	108	50	50.4	2197	2255	34
78.0	−67.5	108	50	50.4	2287	2286	95
81.0	−67.5	108	50	50.4	2263	2298	58
84.0	−67.5	108	50	50.4	2281	2305	70
87.0	−67.5	108	50	50.4	2261	2310	44
90.0	−67.5	108	50	50.4	2279	2282	90

[a] Total observed events: 20,067; total background events: 20,105.
[b] Total observed events: 49,246; total background events: 49,258.

this they derive a gamma-ray intensity above 100 MeV from the LMC as 2.3×10^{-7} cm^{-2} s^{-1}. This flux arises from synchrotron scattering of gamma-ray photons from point sources on cosmic rays within the LMC. If this emission extends into the UHE region with a differential index of -2, the flux becomes 3.5×10^{-13} cm^{-2} s^{-1} at energies greater than 65 TeV. From Table 4, our upper limit on the total gamma-ray emission above 65 TeV from the LMC is 1.8×10^{-12} cm^{-2} s^{-1}. While not severely constraining the theoretical models, our upper limit is consistent with the calculations of Fichtel et al. (1991).

5. DISCUSSION

From observations using the JANZOS Cerenkov facility at large zenith angles we have obtained stringent upper limits on the UHE flux from SMC X-1 and SN 1987A. The object LMC X-4 was observed at zenith angles around 72°, which were the largest for these observations. The upper limit on the flux from LMC X-4 was not as stringent as those obtained for the other objects, mainly because of the poor angular resolution at zenith angles greater than 70°. Such zenith angles probably represent the limit of the large zenith angle technique for this experiment.

TABLE 4

UPPER LIMITS[a] ON TOTAL UHE EMISSION FROM MAGELLANIC CLOUDS

Galaxy	Threshold Energy (TeV)	Integral Flux Upper Limit (10^{-13} cm^{-2} s^{-1} msr^{-1})	Luminosity Upper Limit (10^{37} ergs s^{-1} msr^{-1})
SMC.....	30	19.3	18.4
LMC.....	65	1.8	2.3

[a] At 95% confidence level.

Each of the objects SMC X-1, PSR 0540−693, SN 1987A, and LMC X-4 showed positive excesses, although they were all statistically insignificant. The results reported here for these objects provide motivation for further, more sensitive observations. The JANZOS air-shower array has been operating since 1987 October. The analysis of the full data base is expected to provide more sensitive measurements on the steady state UHE gamma-ray flux from these objects.

The excess detected from the direction of LMC X-4 may be of statistical origin. Transient effects of this magnitude and time duration cannot be detected with air-shower arrays currently operating in the Southern Hemisphere. For example, the cosmic-ray event collection rate for the JANZOS air-shower array in a $3° \times 2°$ ($\alpha \times \delta$) window in the LMC region is of the order of 1 hr^{-1}. The large effective area enjoyed by taking the Cerenkov technique to large zenith angles enabled at least 100 events to be recorded from the direction of LMC X-4 in a 4.6 hr observation period. An opportunity for further studies of

transient emission from LMC X-4 and other southern objects may be provided by the CANGAROO telescope in Australia (Hara 1990), which employs the imaging technique. The application of this method at large zenith angles presents an interesting proposition.

Since they are relatively close, the Magellanic Clouds provide suitable subjects for investigating various aspects of cosmic-ray physics in galaxies other than our own. The observations presented here show no evidence at all that these galaxies as a whole are sources of UHE gamma rays at intensities above our detection threshold.

We are grateful to Professors J. Arafune and H. Sugawara for their support. We acknowledge D. Robinson for his hospitality at the Black Birch site. We appreciate the cooperation of the New Zealand Ministry of Works and Development (Blenheim Branch). This work is supported in part by a Grant-in-Aid for Scientific Research from the Ministry of Education, Science, and Culture; the Yamada Foundation; the Inoue Foundation; the Japan-New Zealand Foundation; the University of Auckland Research Committee; the University of Auckland Finance Committee; the New Zealand Scientific Research Distribution Committee; the New Zealand University Grants Committee; the Australian Department of Industry, Technology, and Commerce; and the Donovan Foundation.

REFERENCES

Allen, W. H., et al. 1991, (The JANZOS Collaboration). 1992, Proc. 22d, Int. Cosmic-Ray Conf. (Dublin), 1, 376
Bell, A. R. 1978a, MNRAS, 182, 147
———. 1978b, MNRAS, 182, 443
Berezinsky, V. S., & Prilutsky, O. F. 1978, A&A, 66, 325
Berezinsky, V. S., & Stanev, T. 1989, Phys. Rev. Lett., 63, 1035
Blandford, R. D., & Ostriker, J. P. 1978, ApJ, 221, L29
Bond, I. A., et al. (The JANZOS Collaboration). 1988, Phys. Rev. Lett., 61, 2292
Bond, I. A., et al. (The JANZOS Collaboration). 1989, ApJ, 344, L17
Bond, I. A., et al. (The JANZOS Collaboration). 1990, Proc. 21st Int. Cosmic-Ray Conf. (Adelaide), 2, 210
Brazier, K. T. S., et al. 1990, Proc. 21st Int. Cosmic-Ray Conf. (Adelaide), 2, 300
Chadwick, P. M., et al. 1988, ApJ, 333, L19
Chadwick, P. M., McComb, T. J. L., & Turver, K. E. 1990, J. Phys. G, 16, 1773
Chanmugam, G., & Brecher, K. 1985, Nature, 313, 767
Cheng, K. S., & Ruderman, M. 1989, ApJ, 337, L77
Cheng, K. S., Cheung, T., Lau, M. M., Yu, K. N., & Kwok, P. W. 1990, J. Phys. G, 16, 1115
Ciampa, D., Bird, D. J., Clay, R. W., Edwards, P. G., & Protheroe, R. J. 1988, ApJ, 326, L9
Corbet, R. H. D., et al. 1985, MNRAS, 212, 565
Feast, M. W. 1990, in IAU Symp. 148 The Magellanic Clouds and Their Dynamical Interaction with the Milky Way, ed. R. Haynes & D. Milne (Dordrecht: Kluwer), 7
Fichtel, C. E., Özel, M. E., Stone, R. G., & Sreekumar, P. 1991, ApJ, 374, 134
Finnemore, M., et al. 1991, Proc. 22d Int. Cosmic-Ray Conf. (Dublin), 1, 388
Goldreich, P., & Julian, W. H. 1969, ApJ, 157, 869
Gould, R. J., & Rephaeli, Y. 1978, ApJ, 225, 318
Gould, R. J., & Schreder, G. 1966, Phys. Rev. Lett., 16, 252
Greisen, K. 1956, in Progress in Cosmic-Ray Physics, ed. M. A. Wilson (Amsterdam: North-Holland), Vol. 3
Gunn, J. E., & Ostriker, J. P. 1969, Phys. Rev. Lett., 22, 728
Hara, T. 1990, in Astrophysical Aspects of the Most Energetic Cosmic Rays (Singapore: World Scientific), 461
Hillas, A. M. 1982, J. Phys. G, 8, 1475
Hillas, A. M., & Patterson, J. R. 1987, in Very High Energy Gamma-Ray Astronomy, ed. K. E. Turver (Dordrecht: Reidel), 243
Honda, M. 1989, ApJ, 339, 629
Honda, M., Terasawa, T., & Sato, H. 1989, Prog. Theor. Phys., 82, 315
Jelley, J. V. 1966, Phys. Rev. Lett., 16, 479
Levine, A., Rappaport, S., Putney, A., Corbet, R., & Nagase, F. 1991, ApJ, 381, 101
Li, T., & Ma, Y. 1983, ApJ, 272, 317
Lythe, G. D. 1990, M.Sc. thesis, Univ. Auckland
Makino, F. 1988, IAU Circ., Nos. 4530 and 4532
Meyhandan, R., Dawson, B. R., Clay, R. W., Horton, L., Ulrichs, J., & Winn, M. M. 1992, ApJ, 391, 236
Nagase, F. et al. 1990, ApJ, 351, L13
Nakamura, T., Yamada, Y., & Sato, H. 1987, Prog. Theor. Phys., 78, 1065
Primini, F., Rappaport, S., & Joss, P. C. 1977, ApJ, 217, 543
Protheroe, R. J. 1986, MNRAS, 221, 25
Protheroe, R. J., & Clay, R. W. 1985, Nature, 315, 205
Raubenheimer, B. C., North, A. R., De Jager, O. C., & Nel, H. I. 1989, ApJ, 336, 394
Sato, H. 1977, Prog. Theor. Phys., 58, 549
Sembioski, G., & Kertzman, M. P. 1991, Proc. 22d Int. Cosmic Ray Conf. (Dublin), 1, 500
Seward, F. D., Harnden, F. R., & Helfand, D. J. 1984, ApJ, 287, L19
Skinner, G. K., et al. 1982, Nature, 297, 568
Sommers, P., & Elbert, J. W. 1987, J. Phys. G, 13, 553
White, N. E., & Carpenter, G. F. 1978, MNRAS, 183, 11P